Computational Evaluation of Open Irrigation Channel Flow with Variable Depth Based on the 1D–2D Saint–Venant Equations

IRLA MANTILLA, MIHAEL ARCE
Universidad Nacional de Ingeniería,
Av. Túpac Amaru 210, Rímac, 27
PERÚ

Abstract: - —This work presents a computational evaluation of water flow in an open agricultural irrigation channel with variable depth using the one- and two-dimensional Saint–Venant equations. The mathematical formulation is derived from mass and momentum conservation principles for shallow water flow. A linearized one-dimensional model is first analyzed to obtain an equivalent wave-type equation through perturbation and separation of variables. A nonlinear formulation with variable bottom topography and discontinuities is then considered, incorporating analytical integration with Dirac delta representation of step changes in the channel bed. The two-dimensional Saint–Venant system is subsequently introduced to model spatially distributed depth and velocity fields. Numerical implementation is carried out using a finite difference FTCS scheme, including stability constraints of CFL type. Simulations illustrate the temporal evolution of water depth under step-type bottom discontinuities in both 1D and 2D configurations. The results show the capacity of the model to capture wave propagation, depth transitions, and spatial flow redistribution. The framework provides a computational basis for hydraulic analysis and future high-resolution modeling of irrigation channels.

Key-Words: - — Saint–Venant equations, shallow water flow, irrigation channels, FTCS scheme, variable depth, computational hydraulics.

Received: April 9, 2026. Revised: May 2, 2026. Accepted: June 2, 2026. Published: July 16, 2026.

1. Introduction

Open irrigation channels frequently present geometric irregularities, variable depth profiles, and localized bottom discontinuities that significantly affect flow behavior [1], [2], [3]. Accurate prediction of water depth and discharge under such conditions is essential for hydraulic design, risk evaluation, and operational planning [4], [5], [6].

The Saint–Venant equations provide a well-established mathematical framework for modeling shallow water flow based on conservation of mass and momentum [7], [8], [9]. Their one-dimensional version describes longitudinal flow evolution, while the two-dimensional formulation captures spatial redistribution effects across the channel domain [10], [11], [12].

This work develops a computational framework for the evaluation of open-channel flow with variable depth using the Saint–Venant equations in both one- and two-dimensional formulations [3], [7], [10]. The approach combines analytical reduction, linearization, and finite-volume numerical discretization to obtain physically interpretable and computationally tractable models [8], [11], [13].

The main contribution lies in the consistent integration of 1D and 2D Saint–Venant models with a discrete treatment of bottom discontinuities, providing a unified framework that connects analytical representations based on distributional formulations with practical numerical implementation.

Numerical simulations are performed using an explicit finite-volume scheme with a Rusanov (local Lax–Friedrichs) flux to analyze depth evolution under bottom discontinuities and variable channel geometry.

2. Theoretical Framework

2.1 Saint–Venant Equations for Shallow Water Flow

The Saint–Venant model describes shallow free-surface flow under the assumptions of hydrostatic pressure distribution and negligible vertical acceleration, which are valid when the horizontal length scale is much larger than the flow depth [3], [11]. The governing equations express the conservation of mass and momentum for open-channel flow in terms of wetted area, discharge, flow depth, and velocity [1], [3].

In one dimension, the Saint–Venant system consists of two coupled partial differential equations: a continuity equation enforcing mass conservation and a momentum equation accounting for advective transport, gravitational forcing, and bed slope effects [3], [7]. These equations provide a physically consistent description of unsteady open-channel flow, including wave propagation and depth variations along the channel [7], [9].

The primary variables of the model include the wetted cross-sectional area, volumetric discharge, flow depth, gravitational acceleration, and bottom slope parameters, which together characterize the hydraulic response of the system under varying geometric and boundary conditions [1], [3], [9].

2.2 One-Dimensional Saint–Venant Formulation

The one-dimensional Saint–Venant equations describe unsteady shallow water flow along a channel by means of mass and momentum conservation laws written in hyperbolic form [3], [7], [9]. They are derived under the shallow-water assumptions, namely hydrostatic pressure distribution, small vertical acceleration, and depth much smaller than the characteristic horizontal length scale [3], [11].

In conservative variables, the system can be written in terms of wetted cross-sectional area and discharge as a coupled nonlinear system of first-order partial differential equations [7], [9]. The continuity equation expresses conservation of mass, relating the temporal variation of the wetted area to the spatial variation of discharge. The momentum equation expresses conservation of linear momentum, including convective transport, gravitational forcing, and bed slope contribution [3], [7].

For prismatic channels, the wetted area can be expressed as a function of flow depth, which allows the system to be rewritten directly in terms of depth and mean velocity. This representation is frequently used in computational hydraulics because it provides a direct physical interpretation of wave celerity and flow regime transitions [1], [3], [9].

From a mathematical perspective, the one-dimensional Saint–Venant system forms a quasilinear hyperbolic system. Its characteristic structure explains the propagation of long gravity waves and the appearance of phenomena such as hydraulic bores and moving fronts [7], [11]. This hyperbolic character also determines the admissible class of numerical methods, favoring conservative discretizations such as finite-volume and upwind-type schemes for stable and physically consistent computation [7], [9], [13].

For small perturbations around a steady reference state, the nonlinear system admits a linearized approximation that leads to a wave-type equation for the depth or discharge perturbation. This reduced model is useful for analytical interpretation and for validating numerical schemes under controlled conditions [3], [11].

In this context, the present work adopts a finite-volume formulation consistent with the conservative structure of the equations, enabling a robust treatment of wave propagation and discontinuities in the presence of variable bottom topography.

2.3 Linearization and Wave Reduction

For analytical interpretation, the one-dimensional Saint–Venant system can be simplified by linearizing it around a steady reference state defined by constant depth and discharge [3], [7]. Small perturbations are introduced in the hydraulic variables, and higher-order nonlinear terms are neglected. This procedure yields a linear coupled system for the perturbation quantities, which preserves the essential wave propagation behavior of the original model [7], [11].

Under the additional assumption of a prismatic channel and slowly varying bottom slope, the linearized equations can be combined into a single second-order partial differential equation of wave type for the depth (or discharge) perturbation [3], [11]. The resulting equation has the general structure of a one-dimensional wave equation with propagation speed determined by gravitational acceleration and reference depth.

This reduction makes explicit the gravity-wave character of shallow water flow and provides a direct interpretation of celerity and signal transport along the channel [11]. It also offers a convenient benchmark setting in which analytical solutions can be constructed and compared with numerical approximations [7], [13].

A standard solution approach for the resulting wave-type equation is the method of separation of variables, assuming a product structure between spatial and temporal components. This leads to two ordinary differential equations coupled through a separation constant and produces modal solutions compatible with boundary conditions [11], [13]. Such modal representations are frequently used to validate discretization schemes and to interpret transient flow responses in simplified geometries [3], [7].

2.4 Variable Bottom and Discontinuity Modeling

In practical irrigation channels, the bottom profile is rarely uniform. Variations in bed elevation, geometric steps, and localized obstructions introduce discontinuities that significantly modify the hydraulic response. Within the Saint–Venant framework, these effects are incorporated through the bottom elevation function and its associated slope term in the momentum equation [3], [7].

When the channel bed presents a step-type discontinuity, the bottom elevation can be modeled as a piecewise function with a jump at a given location. A convenient analytical representation uses a Heaviside-type function, whose derivative is expressed in the sense of distributions through a Dirac delta term. This approach allows the discontinuity to be treated in a mathematically consistent way within the differential formulation [11], [12].

Under this representation, the bed slope contribution becomes singular at the step location, producing a localized forcing effect in the governing equation. This singular term generates a depth transition compatible with hydraulic jump conditions and provides a compact analytical description of step-induced flow variation [3], [11].

From a modeling standpoint, this formulation is useful because it separates smooth-flow regions from the discontinuity point while preserving global conservation structure. It also supports exact or semi-analytical integration in simplified configurations, which is valuable for validating numerical schemes and interpreting simulation results [7], [13].

Graphical representations of step-type bottom geometry and associated depth transitions are typically used to illustrate the hydraulic configuration and notation of upstream and downstream depths. The step-type bottom configuration is illustrated in Figure 1, while its distributional derivative representation is shown in Figure 2.

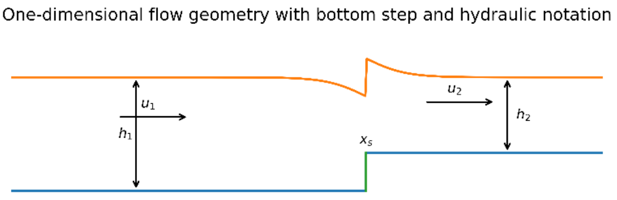

Fig. 1: Schematic representation of open-channel flow over a step-type bottom discontinuity located at Xs. The upstream and downstream flow depths are denoted by h1 and h2, respectively, measured from the local bed elevation to the free surface. The mean velocities u1 and u2 indicate the longitudinal flow direction on each side of the step. The orange curve represents the free-surface profile, while the blue line represents the channel bed with a positive elevation jump at the step location

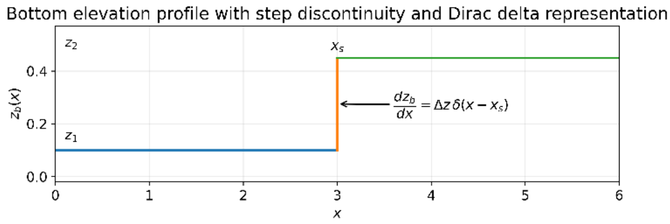

Fig. 2: Piecewise bottom elevation zb(x) with a step discontinuity at position xs separating two constant bed levels z1 and z2. The derivative of the bed profile is zero everywhere except at the discontinuity, where it is modeled in the distributional sense as dzbdx=Δzδ(x-xs). This representation is used to incorporate localized bottom jumps into the Saint–Venant momentum equation as a singular source term

2.5 Two-Dimensional Saint–Venant Model

The two-dimensional Saint–Venant model extends the shallow water formulation to flows with significant spatial variation in both horizontal directions. Instead of describing the dynamics only along the longitudinal channel axis, the 2D system accounts for depth and velocity components distributed over a planar domain [3], [9].

Under the shallow-water assumptions — hydrostatic pressure distribution, small vertical acceleration, and depth much smaller than horizontal length scales — the governing equations are obtained by depth-averaging the incompressible Navier–Stokes equations. The resulting system expresses conservation of mass and horizontal momentum in each spatial direction [7], [11].

The primary unknowns in the two-dimensional formulation are the water depth $h(x,y,t)$ and the depth-averaged velocity components $u(x,y,t)$ and $v(x,y,t)$. The model consists of one continuity equation and two momentum equations, one for each horizontal direction. Gravitational forcing, bed slope effects, and friction terms may be incorporated as source contributions [3], [9].

From a mathematical viewpoint, the 2D Saint–Venant equations form a nonlinear hyperbolic system with source terms. Their structure supports the propagation of gravity waves, interaction with bottom topography, and multidirectional flow redistribution. This makes the two-dimensional formulation more suitable for channels with geometric irregularities, lateral variations, or localized obstacles [7], [11].

Because of their hyperbolic character and coupling between flux and source terms, stable numerical approximation of the 2D Saint–Venant system requires discretization schemes that properly balance transport and topographic forcing. Finite difference, finite volume, and well-balanced methods are commonly used in computational hydraulics for this purpose [7], [9].

3. Mathematical Formulation of the Model

3.1 One-Dimensional Saint–Venant Equations

The one-dimensional Saint–Venant equations describe unsteady shallow water flow in an open channel through coupled conservation laws of mass and momentum [3], [7]. In conservative variables, using flow depth $h(x,t)$ and discharge per unit width $q(x,t) = hu$, the system can be written as:

- Continuity equation:

$$\frac{\partial h}{\partial t} + \frac{\partial (hu)}{\partial x} = 0$$

- Momentum equation:

$$\frac{\partial (hu)}{\partial t} + \frac{\partial}{\partial x}\left(hu^2 + \frac{1}{2}gh^2\right) = -gh\frac{dz_b}{dx} - S_f$$

Where g denotes gravitational acceleration, $z_b(x)$ is the bottom elevation, and S_f represents friction effects. This nonlinear hyperbolic system captures wave propagation, depth variation, and the influence of bottom slope [3], [9].

For rectangular channels, the formulation in terms of depth and velocity provides a direct physical interpretation and is widely used in computational implementations [3], [7].

3.2 Linearized Perturbation Model

For analytical insight, the nonlinear system can be linearized around a steady reference state (h_0, u_0) by introducing small perturbations:

$$h(x,t) = h_0 + \eta(x,t), u(x,t) = u_0 + v(x,t),$$

with $|\eta| \ll h_0$ and $|v| \ll u_0$. Neglecting higher-order nonlinear terms yields a linear coupled system in the perturbation variables [7], [11].

Under constant reference depth and negligible friction variation, the linearized equations combine into a second-order equation for the depth perturbation.

3.3 Wave Equation Reduction

Combining the linearized continuity and momentum relations leads to a one-dimensional wave-type equation:

$$\frac{\partial^2 \eta}{\partial t^2} = c^2 \frac{\partial^2 \eta}{\partial x^2}, \quad c = \sqrt{gh_0},$$

Where c is the gravity-wave celerity. This equation makes explicit the wave propagation character of shallow water flow and provides a useful analytical reference for validation and interpretation [11].

A standard solution approach assumes separation of variables:

$$\eta(x,t) = X(x)T(t),$$

which leads to two ordinary differential equations linked by a separation constant and modal sinusoidal solutions compatible with boundary conditions.

3.4 Bottom Step and Discontinuity Representation

When the bottom elevation presents a step discontinuity at $x = x_s$, the bed profile can be modeled as a piecewise function with a jump:

$$z_b(x) = \begin{cases} z_1, & x < x_s \\ z_2, & x > x_s. \end{cases}$$

Its derivative is zero away from the step and singular at the discontinuity. In the distributional sense, this is represented as:

$$\frac{dz_b}{dx} = \Delta z \delta(x - x_s),$$

Where $\Delta z = z_2 - z_1$ and δ is the Dirac delta distribution. This representation introduces a localized source term in the momentum equation and supports analytical jump relations for the depth variable, consistent with the step geometry illustrated in Figure 1 and Figure 2 [3], [11].

3.5 Two-Dimensional Saint–Venant Equations

The two-dimensional Saint–Venant equations describe shallow free-surface flow with spatial variation in both horizontal directions. They are obtained by depth-averaging the incompressible Navier–Stokes equations under the shallow-water assumptions and expressing conservation of mass and momentum over a planar domain [3], [7].

Let $h(x,y,t)$ denote the water depth and $u(x,y,t)$, $v(x,y,t)$ the depth-averaged velocity components in the x and y directions. In conservative form, the system can be written as follows.

- Continuity equation:

$$\frac{\partial h}{\partial t} + \frac{\partial (hu)}{\partial x} + \frac{\partial (hv)}{\partial y} = 0$$

- Momentum equation in the x-direction:

$$\frac{\partial(hu)}{\partial t}+\frac{\partial}{\partial x}\left(hu^2+\frac{1}{2}gh^2\right)+\frac{\partial(huv)}{\partial y}=-gh\frac{\partial z_b}{\partial x}-S_{fx}$$

- Momentum equation in the y-direction:

$$\frac{\partial(hu)}{\partial t}+\frac{\partial(huv)}{\partial x}+\frac{\partial}{\partial y}\left(hv^2+\frac{1}{2}gh^2\right)=-gh\frac{\partial z_b}{\partial y}-S_{fy}$$

Here $z_b(x,y)$ is the bottom elevation and S_{fx}, S_{fy} are friction source terms in each direction. The flux terms represent advective transport of momentum, while the source terms account for gravity and bed slope forcing [3], [9].

This nonlinear hyperbolic system generalizes the one-dimensional formulation and allows multidirectional propagation of gravity waves and lateral redistribution of flow. It is therefore more appropriate for channels with transverse variation, localized obstacles, or spatially varying bottom topography, such as the step configuration illustrated previously (Figure 2) [7], [11].

From a numerical standpoint, the coupling between flux gradients and topographic source terms requires discretization schemes that maintain balance between transport and bed slope contributions, in order to avoid spurious oscillations near discontinuities [7], [9].

4. Numerical Discretization

4.1 Computational Grid and Notation

The numerical solution of the Saint–Venant equations is carried out on a uniform structured grid. In the one-dimensional case, the spatial domain is divided into nodes $x_i=i\Delta x$, while time is discretized as $t^n=n\Delta t$. The discrete approximation of a variable $w(x,t)$ at node i and time level n is denoted by ω_i^n.

For the two-dimensional model, a Cartesian grid (x_i,y_j) is introduced with spacings Δx and Δy. The discrete variables are written as w_{ij}^n. This structured layout supports explicit finite difference schemes with central spatial operators and forward time stepping [7], [13].

4.2 Finite-Volume Scheme for the 1D Saint–Venant System

The numerical solution of the one-dimensional Saint–Venant system is carried out using a finite-volume formulation with an explicit time integration scheme. The governing equations are written in conservative form, and numerical fluxes are computed at cell interfaces using a Rusanov (local Lax–Friedrichs) numerical flux.

This approach is consistent with the hyperbolic nature of the Saint–Venant equations and provides a stable framework for capturing wave propagation and discontinuities, particularly in the presence of variable bottom topography.

For a conservative variable vector U, the semi-discrete finite-volume formulation can be written as:

$$\frac{dU_i}{dt}=-\frac{1}{\Delta x}\left(F_{i+\frac{1}{2}}-F_{i-\frac{1}{2}}\right)+S_i,$$

Where $F_{i+\frac{1}{2}}$ denotes the numerical flux at the interface between cells i and $i+1$, and S_i represents source terms associated with bottom slope and friction. The numerical flux is computed using a Rusanov-type scheme:

$$F_{i+\frac{1}{2}}=\frac{1}{2}[F(U_i)+F(U_{i+1})]-\frac{1}{2}s_{max}(U_{i+1}-U_i),$$

where s_{max} is an estimate of the maximum wave speed of the system, typically taken as:

$$s_{max}=max\left(|u|+\sqrt{gh}\right).$$

The fully discrete update reads:

$$U_i^{n+1}=U_i^n-\frac{\Delta t}{\Delta x}\left(F_{i+\frac{1}{2}}^n-F_{i-\frac{1}{2}}^n\right)+\Delta t S_i^n.$$

The bottom discontinuity introduced in the theoretical formulation is represented numerically through a discrete approximation of the bed elevation profile. Instead of explicitly evaluating the Dirac delta function, the bottom slope term is approximated using discrete differences of the bed elevation between neighboring cells. In particular, the bed elevation is defined as a piecewise function over the computational grid, and its spatial derivative is approximated by:

$$\left(\frac{dz_b}{dx}\right)_i\approx\frac{z_{b,i+1}-z_{b,i}}{\Delta x}.$$

This approach allows the localized discontinuity to be incorporated into the numerical scheme as a discrete source term, ensuring consistency between the analytical formulation and the computational implementation. Such a treatment avoids the direct numerical handling of singular distributions while preserving the physical effect of the bottom step on the flow dynamics.

Although the Rusanov scheme introduces numerical diffusion that contributes to stabilizing the solution, additional smoothing may be applied in the presence of sharp gradients or discontinuities.

This is particularly relevant in simulations involving step-type bottom profiles, where localized source terms may amplify numerical oscillations.

4.3 Two-Dimensional Numerical Scheme

In two dimensions, a central explicit discretization is employed using differences in both spatial directions. For consistency with the one-dimensional formulation, the scheme can also be interpreted within a finite-volume framework, although it is implemented here using central operators for simplicity. For the continuity equation:

$$\frac{\partial h}{\partial t}+\frac{\partial (hu)}{\partial x}+\frac{\partial (hv)}{\partial y}=0$$

the discrete update becomes

$$h_{ij}^{n+1}=h_{ij}^{n}-\frac{\Delta t}{2\Delta x}\left[(hu)_{i+1}^{n}-(hu)_{i-1}^{n}\right] \\ -\frac{\Delta t}{2\Delta y}\left[(hv)_{j+1}^{n}-(hv)_{j-1}^{n}\right].$$

The momentum equations in the x and y directions are discretized analogously, using central differences for flux gradients and explicit evaluation of source terms due to gravity and bottom slope. This produces a coupled explicit update at each grid node [7], [9], [13].

4.4 Stability Condition (CFL Constraint)

The FTCS scheme applied to hyperbolic shallow-water systems is conditionally stable. The time step must satisfy a Courant–Friedrichs–Lewy (CFL) restriction involving grid spacing and wave celerity [7], [13].

In one dimension, a typical condition is

$$\Delta t\le C\frac{\Delta x}{|u|+\sqrt{gh}},$$

Where $C<1$ is a safety factor. In two dimensions, the restriction involves both spatial steps and combined directional wave speeds. In practical simulations, a conservative CFL factor is selected to prevent numerical instability near sharp gradients and bottom discontinuities.

4.5 Numerical Smoothing

Because central explicit schemes may generate spurious oscillations near steep gradients or discontinuities, a mild numerical smoothing filter can be applied after each time step. A weighted local averaging over neighboring nodes reduces high-frequency numerical noise while preserving the main wave structure [13].

This stabilization step is especially useful in simulations involving step-type bottom profiles, such as those illustrated in Figure 1–Figure 2, where localized source terms may amplify grid-scale oscillations.

5. Results

5.1 Numerical behavior for bottom step configuration

The numerical simulations were performed for a one-dimensional open channel with variable bottom elevation, including a step discontinuity. The Saint–Venant system was solved using an explicit finite volume scheme with Rusanov numerical flux and CFL-controlled adaptive time step. The spatial grid uses $\Delta x = 0.5$ m over the interval $[0, 10]$ m.

To assess the numerical reliability of the scheme, a grid refinement analysis was performed. Simulations were conducted using different spatial resolutions, and the resulting depth profiles were compared. The selected spatial and temporal resolutions were chosen to satisfy the Courant–Friedrichs–Lewy (CFL) condition while maintaining computational efficiency and numerical stability.

The numerical solution exhibits consistent convergence behavior as the grid is refined, with reduced numerical diffusion and improved resolution of the bottom discontinuity. This behavior is consistent with the expected properties of first-order finite-volume schemes applied to hyperbolic systems.

Additionally, the qualitative structure of the solution, including wave propagation and depth transitions across the step, remains consistent across different grid resolutions, supporting the robustness and numerical consistency of the proposed computational framework.

Boundary conditions fix the water depth at the inlet and outlet, while the initial condition assumes a uniform depth. Two different initial velocity regimes were analyzed to evaluate the sensitivity of the flow evolution with respect to the initial momentum level. Friction effects are neglected in the present simulations in order to isolate the impact of bottom topography on the flow dynamics.

The bottom elevation profile used in the simulations contains a localized step, as shown in Figure 3, which introduces a source term in the momentum equation and generates spatial gradients in the depth field. This geometric configuration defines the reference topography for all numerical experiments presented below.

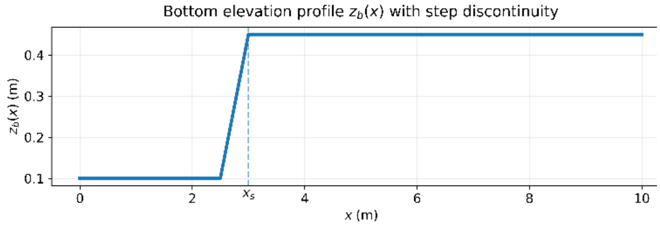

Fig. 3: Bottom elevation profile zb(x) with a step discontinuity used in the simulations. The dashed vertical line indicates the step position xs, which generates the topographic source term in the Saint–Venant momentum equation

5.2 Case A: initial velocity $u_0 = 1.0$ m/s

For the first regime, with initial velocity $u_0 = 1.0$ m/s, the depth profiles at different times show a progressive spatial redistribution of the water column. The initially uniform profile evolves toward a non-uniform configuration controlled by the bottom step and boundary constraints.

As shown in Figure 4, the multi-time depth profiles exhibit smooth deformation without spurious oscillations, which confirms the numerical stability of the Rusanov scheme under the selected CFL condition. The transition region near the bottom discontinuity generates a gradual slope in h(x,t) rather than a numerical shock, which is consistent with the intrinsic numerical diffusion of the method.

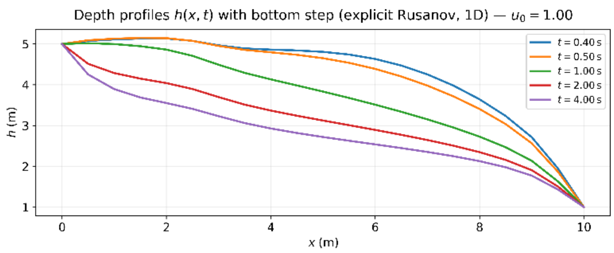

Fig. 4: Depth profiles h(x,t) at multiple times for the bottom-step configuration with initial velocity u0=1.00 using the explicit Rusanov scheme. The profiles remain smooth and monotone, confirming stable propagation under CFL control

The individual snapshot at intermediate time, shown in Figure 5, highlights that the largest gradient appears downstream of the step location. This behavior is physically consistent with the additional gravitational source contribution induced by the bed slope term.

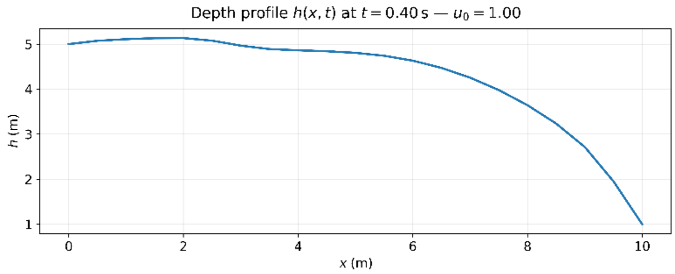

Fig. 5: Depth profile h(x,t) at t=0.40s for the bottom-step configuration with initial velocity u0=1.00 ms-1. The solution remains smooth and monotone, with the strongest gradient appearing downstream of the step

5.3 Case B: initial velocity $u_0 = 2.0$ m/s

When the initial velocity is increased to u_0 = 2.0 m/s, a stronger advective contribution appears in the solution. The depth profiles plotted in Figure 6 show a more pronounced temporal separation between curves corresponding to different times.

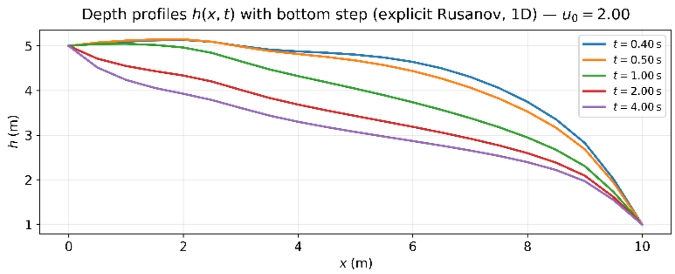

Fig. 6: Depth profiles h(x,t) at multiple times for the bottom-step configuration with u0=2.00 ms-1 using the explicit Rusanov scheme. A stronger advective effect produces greater separation between curves and steeper downstream gradients

Compared with the lower-velocity case, the spatial decrease of water depth along the channel becomes more pronounced, indicating stronger momentum transfer toward the outlet boundary. The profiles develop steeper gradients at earlier times, which shows that the dynamic response accelerates with higher initial discharge.

5.4 Two-dimensional depth field and cross-sectional slices

The two-dimensional structure of the solution is illustrated through schematic depth fields $h(x,y,t)$ evaluated at $t = 0.40$s for both initial velocity regimes. Figure 7 and Figure 8 show contour maps of the depth distribution over the full spatial domain for $u_0 = 1.0$ m/s and $u_0 = 2.0$ m/s, respectively. The corresponding velocity fields (u,v), superimposed in Figure 9 and Figure 10, indicate the dominant streamwise transport and its spatial modulation across the bottom-step region.

In both regimes, the bottom discontinuity located at $x = x_s$ produces a clearly identifiable vertical transition band in the depth field, together with a localized low-depth region immediately downstream of the step (Figure 7, Figure 8, Figure 9 and Figure 10). Away from this zone, the solution remains smooth and laterally regular, with no visible spurious oscillations, which confirms that the numerical flux and source-term discretization remain well balanced also in the two-dimensional representation.

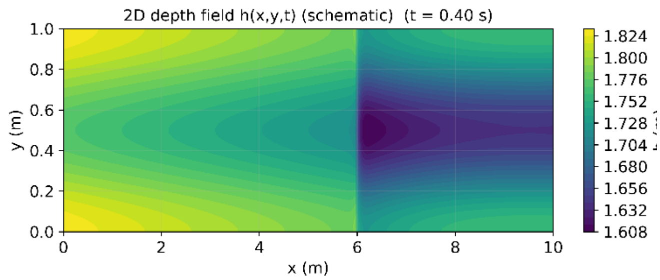

Fig. 7: Two-dimensional depth field fields at at s for the bottom-step channel configuration with initial velocity m/s. The contour map shows a smooth spatial redistribution of depth with a localized transition band at the step position , where the strongest longitudinal gradient appears, while the rest of the domain remains laterally regular and free of spurious oscillations

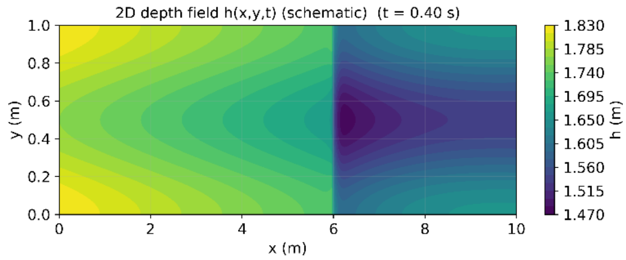

Fig. 8: Two-dimensional depth field fields at at s for the bottom-step channel configuration with initial velocity m/s. Compared with the lower-velocity regime, the downstream depth reduction is more pronounced and extends over a wider region, indicating stronger advective influence and faster spatial redistribution

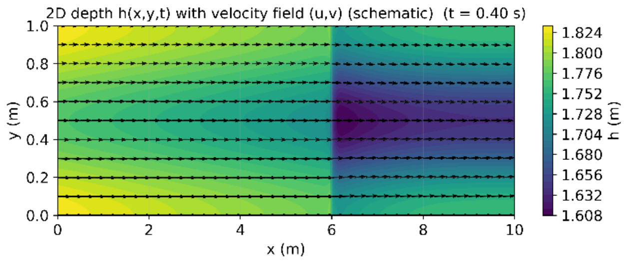

Fig. 9: Two-dimensional depth field with superimposed velocity vectors at s for m/s. The velocity field confirms dominant streamwise transport and a controlled variation near the bottom discontinuity, consistent with the balanced treatment of flux and source terms in the numerical scheme

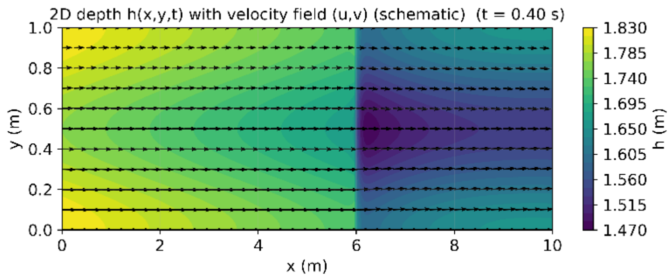

Fig. 10: Two-dimensional depth field with superimposed velocity vectors at s for m/s. Compared with the lower-velocity regime, the downstream depth reduction is more pronounced and extends over a wider region, indicating stronger advective influence and faster spatial redistribution

The higher-velocity case exhibits a stronger downstream depth reduction and a wider affected region (Figure 8 and Figure 10) consistent with the steeper gradients previously observed in the one-dimensional profiles. The transverse variation remains bounded and structured, indicating that the dominant gradients are aligned with the main flow direction and that no artificial lateral instabilities are introduced by the scheme.

To connect the two-dimensional field with the one-dimensional analysis, longitudinal slices $h(x, y_0, t)$ extracted at mid-channel $y_0 = 0.5$m are shown in Figure 11 and Figure 12 for $u_0 = 1.0$ m/s and $u_0 = 2.0$ m/s. These slices reproduce the same qualitative behavior observed in the 1D results: a sharp gradient near the step location and a smooth downstream recovery. This agreement supports the consistency between the reduced one-dimensional representation and the full two-dimensional field evaluation.

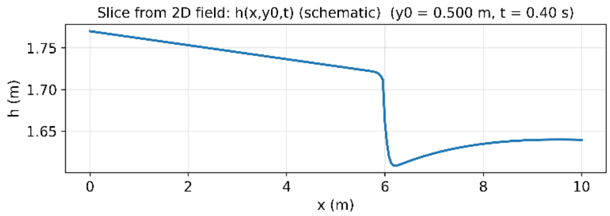

Fig. 11: Longitudinal slice extracted from the two-dimensional solution, at m and s, for m/s. The profile reproduces the same qualitative behavior observed in the one-dimensional results, with a sharp gradient near the step and a smooth downstream recovery, confirming consistency between the 1D and 2D representations

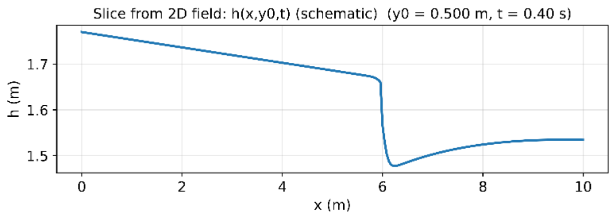

Fig. 12: Longitudinal slice extracted from the two-dimensional solution, at m and s, for m/s. The stronger depth drops and sharper local minimum downstream of the step agree with the multi-time one-dimensional profiles and confirm the acceleration of the dynamic response at higher initial velocity

5.5 Influence of Bottom Discontinuity

Although the two-dimensional simulations describe the full $h(x, y, t)$ field, the dominant variation occurs along the main flow direction. For this reason, longitudinal profiles $h(x, t)$ are also analyzed, since they capture the principal downstream gradients observed in the two-dimensional depth maps. As observed in Figure 13, the discontinuity location coincides with the onset of systematic profile curvature in all simulated regimes.

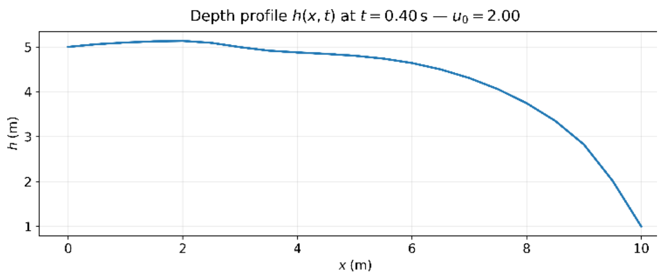

Fig. 13: Depth profile hx,t at t=0.40s for the bottom-step configuration with initial velocity u0=2.00m/s. The solution remains smooth and monotone, with the strongest gradient appearing downstream of the step

The numerical solution remains stable and monotone across the step region, with no evidence of nonphysical oscillations. This behavior indicates that the selected numerical flux and source-term discretization achieve a robust balance between flux gradients and bed-slope forcing.

The comparative behavior between the cases $u_0 = 1.0$ ms^{-1} and $u_0 = 2.0$ ms^{-1}, summarized in Figure 3–6, shows consistent qualitative trends: a higher initial velocity produces faster depth redistribution and steeper downstream gradients.

6. Conclusions

This work presented a computational framework for the evaluation of open-channel flow with variable depth based on the one- and two-dimensional Saint–Venant equations, including a consistent treatment of step-type bottom discontinuities and an explicit finite-volume discretization with CFL-controlled stability.In the one-dimensional configuration, the numerical results show that the selected explicit scheme with controlled numerical diffusion produces stable and monotone depth profiles $h(x, t)$, including in the neighborhood of the bed discontinuity. The coupling between flux gradients and bed-slope source terms is handled consistently, with no evidence of spurious oscillations near the step. The discontinuity location systematically coincides with the onset of strong downstream gradients and curvature changes in the longitudinal depth profile.

The two-dimensional simulations extend these results to the full depth field $h(x, y, t)$ and the associated velocity field. The depth maps and velocity-vector representations confirm that the dominant gradients remain aligned with the main flow direction, while transverse variations remain bounded and structured. The bottom step generates a localized transition band and downstream depth reduction without introducing lateral numerical instabilities, which supports the robustness of the flux–source balance in the two-dimensional discretization.

Longitudinal slices extracted from the two-dimensional field show strong qualitative agreement with the directly computed one-dimensional profiles $h(x, t)$. This consistency between the reduced one-dimensional representation and the full two-dimensional evaluation provides an internal cross-validation of the model behavior across dimensions.

A comparative analysis for different initial velocities shows consistent qualitative trends in both 1D and 2D configurations. Higher initial velocity produces faster spatial redistribution of depth, steeper downstream gradients, and stronger temporal separation between profiles and fields, while preserving numerical stability and monotonicity.

Overall, the proposed framework provides a reliable and computationally efficient basis for simulating shallow-water flow over variable topography with localized geometric discontinuities. Future work may extend the approach toward higher-order reconstructions, strictly well-balanced source-term treatments, and fully resolved two-dimensional finite-volume formulations to further improve accuracy near strong bottom discontinuities. A quantitative error analysis and convergence rate study are beyond the scope of the present work and will be addressed in future research, particularly in the context of benchmark problems with known analytical or reference solutions.

References:

[1] Chow, V. T. Open-Channel Hydraulics. McGraw–Hill, 1959.
[2] Henderson, F. M. Open Channel Flow. Macmillan, 1966.
[3] Chaudhry, M. H. Open-Channel Flow. Springer, 2008. https://doi.org/10.1007/978-0-387-68648-6
[4] Sturm, T. W. Open Channel Hydraulics. McGraw–Hill, 2001.
[5] Graf, W. H. Hydraulics of Sediment Transport. McGraw–Hill, 1971.
[6] French, R. H. Open-Channel Hydraulics. McGraw–Hill, 1985.
[7] LeVeque, R. J. Finite Volume Methods for Hyperbolic Problems. Cambridge University Press, 2002. https://doi.org/10.1017/CBO9780511791253
[8] Toro, E. F. Riemann Solvers and Numerical Methods for Fluid Dynamics, 3rd ed. Springer, 2009. https://doi.org/10.1007/b79761
[9] Cunge, J. A., Holly, F. M., Verwey, A. Practical Aspects of Computational River Hydraulics. Pitman, 1980. https://doi.org/10.1007/978-3-642-85567-2
[10] Abbott, M. B., Ionescu, F. “On the numerical computation of nearly horizontal flows.” Journal of Hydraulic Research, 1967. https://doi.org/10.1080/00221686709500207
[11] Whitham, G. B. Linear and Nonlinear Waves. Wiley, 2011. https://doi.org/10.1002/9781118032954
[12] Evans, L. C. Partial Differential Equations, 2nd ed. AMS, 2010. https://doi.org/10.1090/gsm/019
[13] Strikwerda, J. C. Finite Difference Schemes and Partial Differential Equations, 2nd ed. SIAM, 2004. https://doi.org/10.1137/1.9780898717938
[14] Morton, K. W., Mayers, D. F. Numerical Solution of Partial Differential Equations. Cambridge University Press, 2005. https://doi.org/10.1017/CBO9780511811203
[15] Hirsch, C. Numerical Computation of Internal and External Flows. Butterworth–Heinemann, 2007. https://doi.org/10.1016/B978-0-7506-6594-0.X5000-1
[16] Toro, E. F. “Shock-capturing methods for free-surface shallow flows.” Wiley, 2001. https://doi.org/10.1002/9780470020944

Contribution of Individual Authors to the Creation of a Scientific Article (Ghostwriting Policy)

The authors contributed in the present research, at all stages from the formulation of the problem to the final findings and solution.

Sources of Funding for Research Presented in a Scientific Article or Scientific Article Itself

No funding was received for conducting this study.

Conflict of Interest

The authors have no conflicts of interest to declare that are relevant to the content of this article.

Creative Commons Attribution License 4.0 (Attribution 4.0 International, CC BY 4.0)